PCCP

ROYAL SOCIETY OF CHEMISTRY

PAPER

View Article Online
View Journal | View Issue

Cite this: *Phys. Chem. Chem. Phys.*, 2023, **25**, 27836

Solid state ^{1}H, ^{7}Li, and ^{13}C NMR studies on new ionic plastic crystals of crown ether–Li-TFSA complexes†

Akira Kobayashi,[a] Jun Yamagami,[b] Subham Ranjan,[a] Satoshi Takamizawa[ab] and Hisashi Honda*[ab]

Received 6th June 2023,
Accepted 23rd September 2023

DOI: 10.1039/d3cp02614k

rsc.li/pccp

This study provides the first evidence that a Li ion can form ionic plastic crystals using crown ether with a bis-(trifluoromethanesulphonyl) amide (TFSA) anion. ^{1}H, ^{7}Li, and ^{13}C nuclear-magnetic-resonance (NMR) measurements of the 15-crown-5–Li-TFSA complex revealed that the constituents underwent isotropic reorientation in the plastic crystalline phase. The NMR data of the 12-crown-4–Li-TFSA salt showed that the complex is a rotator crystal (the complexes are denoted as [Li 15C5] and [Li 12C4] in this paper). The X-ray diffraction (XRD) reflection patterns of the [Li 15C5] crystal recorded in the highest-temperature solid phase (plastic phase) could be indexed to a cubic structure. Conversely, [Li 12C4] could be fitted to a trigonal structure. In this study, [M (3*n*)C*n*] (M = Li, Na, K; *n* = 4–6) complexes were also prepared, and NMR, DSC, XRD, and electrical conductivity measurements were performed. Based on these results, we additionally revealed that the [Na 15C5] and [K (15C5)$_2$] complexes are also new rotator crystals. Single-crystal XRD measurements also revealed that the [Na 15C5] compound has two stable sites in the crystal. Activation energies of molecular motions in the [M (3*n*)C*n*] crystals were estimated using ^{1}H NMR relaxation time (T_1 and T_2) measurements. The electrical conductivity measurements of [Li 12C4], [Li 15C5], and [Na 15C5] showed high ionic conductivities ($\sim 10^{-2}$ S cm^{-1}).

Introduction

Some compounds (fullerene, adamantane, tetrachloromethane, *etc.*) have a mesophase between the solid and liquid phases,[1–6] although many chemicals (such as H_2O) directly transform from a solid state to a liquid state by heating at ambient pressure. Mesophases can generally be classified into three categories: plastic, rotator, and liquid crystals. In the liquid crystal phase, the orientation of the constituents is ordered; however, their gravity point is disordered (fused). Conversely, in the plastic crystal phase, the orientation of the constituents is disordered in three dimensions and the gravity point is ordered (solidifying). Thus, plastic crystals are often referred to as crystals with liquid characteristics. If the constituents perform an uniaxial rotation in the crystal (orientational disorder in two dimensions), it is called the rotator phase. Owing to the similarities between plastic and rotator crystals, a few researchers treat rotator crystals as plastic crystals. In this literature, the word 'plastic crystal' is distinguished from the rotator crystal. In plastic crystals, the isotropic reorientation motion of constituents results in small entropy changes at the melting point ($\Delta_{mp}S$). A relationship of $\Delta_{mp}S < 21$ J K^{-1} mol^{-1} has been reported (in the literature, $\Delta_{mp}S < 5$ cal deg^{-1} is described),[7] and many plastic crystals satisfy this condition. In addition to isotropic reorientation, the constituents can jump to lattice defects with low activation energies. This translational motion causes plasticity in solid materials. Based on this property, ionic plastic crystals can often be applied in the development of new solid electrolytes as replacements for current organic and polymer solvents. In contrast, there have been scarce reports on the utilization of rotator crystals in the advancement of novel solid electrolytes. It can be considered that the constituents in the rotator phase typically perform translational jumps within a plane perpendicular to the axis of uniaxial rotation (2D diffusion). Bis-(trifluoromethanesulphonyl) amide (TFSA) (Fig. 1) can form ionic liquids with cations.[8–13] Therefore, ionic plastic

[a] *Graduate School of Nanobioscience, Yokohama City University, Kanazawa-ku, Yokohama, 236-0027, Japan*
[b] *Faculty of Science, Yokohama City University, Kanazawa-ku, Yokohama, 236-0027, Japan*

† Electronic supplementary information (ESI) available: Detailed information about thermal, NMR, crystallographic, and electric conductivity studies (pdf). DSC data: Fig. S1. ^{1}H NMR spectra: Fig. S2. ^{13}C NMR spectra: Fig. S3. Crystallographic data: Fig. S4. Electrical conductivity: Fig. S5. CCDC 2237016 and 2265322. For ESI and crystallographic data in CIF or other electronic format see DOI: https://doi.org/10.1039/d3cp02614k

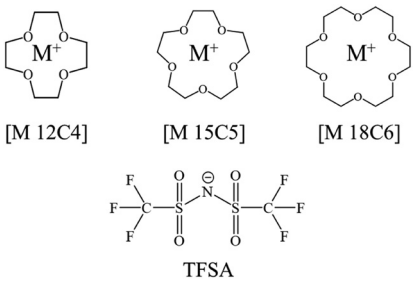

Fig. 1 Chemical structures treated in this study (M = Li, Na, and K).

crystals have been investigated in TFSA salts with alkylammonium, bis-quaternary ammonium, pyrrolidinium, *etc.*[14–16] It has also been reported that ionic conductivities reach 10^{-2} S cm^{-1} when a Li-TFSA salt is doped into plastic crystals, ionic liquids, polymers, *etc.*[17–22]

Many researchers have actively developed ionic conductors using plastic crystals; however, plastic crystals formed by alkali metal ions have been rarely reported without MNO_2 (M = K, Rb, and Cs).[23–26] We have proposed that both globular cations and anions undergo isotropic reorientation if the Coulomb force acting among the ions is sufficiently weak, similar to a molecular plastic crystal. Based on this idea, we have found many new ionic plastic crystals in tetraalkylammonium salts[26–31] and 4-aza-1-azoniabicyclo[2.2.2]octane, 1-alkyl (denoted as [N-R DABCO], R = Me, Et) compounds[32] with $[BEt_3Me]^-$ and $[BEt_4]^-$ counter anions. Here, the alkyl groups of the cation and anion act as spacers between the N and B atoms which can be assumed to be the centres of charge. In addition, a novel chemical family of $[n\text{-}C_xH_{(2x+1)}NEt_3][BEt_3Me]$, which has plastic ($x$ = 1–5), rotator (x = 6, 7), and ionic liquid crystals ($8 \leq x \leq 16$), has been developed.[33] Based on this proposal, it is expected that plastic crystals constructed using alkali metal ions can be obtained if a clathrate compound with alkali metal ions is prepared.

It is well known that crown ethers can form complexes with alkali metal ions. Abu-Lebdeh *et al.* reported that Li-TFSA salts form ionic plastic crystals with crown ethers of 12-crown-4 and 18-crown-6[34] (We have abbreviated [(3*n*)-crown-*n* ether–M-TFSA] complexes as [M (3*n*)C*n*] (M = Li, Na, K; n = 4–6) in this paper, *e.g.* [Li 12C4], [Li 18C6], and [K $(12C4)_2$]). Abu-Lebdeh *et al.* based their assignment of plastic crystals only on the DSC results: $\Delta_{mp}S$ values of 44.5 J K^{-1} mol^{-1} at 418 K ([Li 12C4]) and 4.5 J K^{-1} mol^{-1} at 332 K ([Li 18C6]). The former is larger than the proposed value of 21 J K^{-1} mol^{-1}; however, the authors explained that the flexibility of the anion chains results in a large $\Delta_{mp}S$ value.[34] Another research group measured the IR spectra, Raman spectra, DSC curves, and ionic conductivities of [Li 12C4], [Li 15C5], and [Li 18C6].[35] These studies show that [Li 12C4] and [Li 18C6] crystals have a high ionic conductivity of $10^{-5} \sim 10^{-4}$ S cm^{-1}; however, no information about molecular motions has been reported. An essential characteristic of plastic crystals is 'isotropic reorientation'; hence, the utilization of nuclear magnetic resonance (NMR) data is imperative for investigating plastic crystals.

In this study, solid-state ^{1}H, ^{7}Li, and ^{13}C NMR spectra and relaxation times were measured as a function of temperature in powdered samples of [M (3*n*)C*n*] (M = Li, Na, K; n = 4–6) salts to obtain information on molecular motions. In the case of solid-state ^{1}H NMR spectra, information about the interactions among the constituents is obtained because the line widths of the signals are mainly determined by dipole–dipole interactions between the ^{1}H nuclei. The line breadth is frequently estimated using the second moment of the spectrum (M_2). A relationship of $M_2 < 1$ G^2 is often reported in plastic crystals because of the constituents' jump to lattice defects in addition to isotropic reorientation.[36,37] The ^{1}H NMR spin–lattice relaxation time (T_1) and spin–spin relaxation time (T_2) provided information about the motion frequencies and diffusion of the constituents, respectively. In the case of the ^{7}Li nucleus (I = 3/2), a central transition signal accompanied by two satellite peaks beside itself (a first-order line pattern of a nucleus with I = 3/2) can be recorded in ordinal crystals.[38] However, it can be expected that a ^{7}Li signal without satellite peaks is detected in plastic crystals (the quadrupole coupling constant (QCC) is zero) because the isotropic reorientation of the constituents results in an isotropic electric field gradient (EFG) at the nucleus. In solid-state ^{13}C NMR spectra of ordinal compounds, line shapes with chemical shift anisotropy (CSA) are generally recorded. However, averaging the three components of the chemical shift (CS) tensor (σ_{xx}, σ_{yy}, and σ_{zz}) results in a Lorentz-type line shape in the spectrum if the constituents exhibit isotropic reorientation in the crystal (plastic phase). Solid-state NMR measurements of other crown ether complexes have been reported, including ^{13}C CP/MAS (CP: cross-polarisation and MAS: magic angle spinning) NMR absorption curves of 18-crown-6 crystals and 18-crown-6–2LiOPh, –NaNCS·H_2O, and –KSCN complexes,[39] and ^{7}Li NMR spectra of 12-crown-4–LiCl, –LiBr, and –$LiNO_3$ complexes.[40] The latter literature reveals that a crystal of the 12-crown-4–LiCl complex shows typical ^{7}Li NMR line shapes for first-order quadrupolar interactions with a QCC of 60 kHz at 300 K. Previous studies show that two ^{13}C NMR signals recorded at 69 and 70.5 ppm (240 K) reduced to one signal at 325 K in a crystal of the 18-crown-6–KSCN complex and explain this result in terms of exchange speed between two different conformational structures of the crown ether ring. Based on these data, it is expected that the 12-crown-4–LiCl and 18-crown-6–KSCN complexes do not form plastic crystals. In addition to these two studies, a model of the merry-go-round rotation of crown ether rings has been proposed by ^{2}H NMR measurements of partially deuterated 15-crown-5–NaI, 15-crown-5–$NaClO_4$, and 21-crown-7–KI solids.[41] In the case of ^{1}H NMR spectra, only a few studies have been reported on crown ether crystals. Gotoh *et al.* reported the narrow solid-state ^{1}H NMR spectra with a M_2 of $\sim$0 for 15-crown-5 and 18-crown-6 with Na and K in graphite intercalation compounds and revealed their molecular dynamics.[42] As described above, NMR spectroscopy is a powerful tool for determining the motional modes of crown ether complexes in crystals.

For our target samples, Shriver *et al.* reported T_{mp} values of 370, 352, and 302 K for [Li 12C4], [Li 15C5], and [Li 18C6],

respectively.[35] By contrast, Abu-Lebdeh *et al.* reported T_{mp} values of 418 and 332 K for [Li 12C4] and [Li 18C6], respectively.[34] Additionally, Shriver *et al.* showed a glass transition at 223 K in the [Li 18C6] crystal; however, this glass transition was not observed in the study reported by Abu-Lebdeh *et al.* (they detected a first-order transition at 243 K). In the case of the other complexes of [M (3*n*)C*n*] (M = Na, K. *n* = 4–6), we could not obtain DSC data; therefore, we prepared complexes of [M (3*n*)C*n*] (M = Li, Na, K; *n* = 4–6) and performed DSC measurements. In this study, we used the symbols T_{tr1} and T_{tr2} to indicate the phase-transition temperatures within the solid phase upon moving from higher to lower temperatures, and the symbols $\Delta_{tr1}S$ and $\Delta_{tr2}S$ at each transition temperature. The characteristics of Phase I, Phase II, *etc.* indicate the solid phase starting from a high temperature.

X-ray diffraction (XRD) measurements of powder and single-crystal samples provide beneficial information for plastic crystal studies because ionic plastic crystals normally have NaCl- and CsCl-type cubic structures (occasionally, tetragonal, trigonal, *etc.*[43]). It has been reported that 12-crown-4 can form not only [Li 12C4] but also [Li $(12C4)_2$].[44] A sandwich structure is also expected in [Na $(12C4)_2$] and [K $(15C5)_2$] because the ionic radii of Na^+ at 95–120 pm and K^+ at 133–144 pm are slightly larger than the cavity radius of 12-crown-4 at 72–81 pm and 15-crown-5 at 86–110 pm, respectively.[45]

In this study, we prepared [M (3*n*)C*n*] (M = Li, Na, K.; *n* = 4–6) and performed solid-state NMR, DSC, XRD, and conductivity measurements.

Results and discussion

DSC

The DSC thermograms of each crown ether complex are plotted in Fig. 2 and Fig. S1 (ESI†). Since plastic crystals frequently have metastable phases, each sample was heated from *ca.* 200 K to just above the melting temperature (the first heating run), successively cooled from the temperature to *ca.* 200 K, and heated again from *ca.* 200 K (the second heating run). Because the same curves as those in the first heating scan were recorded in the second heating run, as displayed in Fig. S1 (ESI†), the phase transition temperatures and enthalpy changes were determined from the data of the second heating scan. The transition temperatures (T_{tr1}, T_{tr2}, ...) and entropy changes ($\Delta_{tr1}S$, $\Delta_{tr2}S$, ...) obtained from the DSC measurements are listed in Table 1. The melting temperatures were checked using test-tube observations. In the case of [Na $(12C4)_2$], [K $(15C5)_2$], and [Li 18C6], these compounds decomposed below each melting temperature. The decomposition temperatures were determined by thermogravimetric (TG) measurements. For [Li 12C4], the DSC curves were similar to those reported for T_{mp} = 418 K, T_{tr1} = 362 K, T_{tr2} = 164 K, and $\Delta_{mp}S$ = 44.5 J K^{-1} mol^{-1}.[34] In the reported studies, these temperatures were estimated by each peak top of the DSC curves; in contrast, we determined the temperatures by each rising edge of each signal. Therefore, a slight difference from the reference value was tolerated. In the case of [Li 18C6], a reference showed endothermic peaks at 243 K, 302 K, and T_{mp} = 322 K;[34] in contrast, another paper reported a glass transition at 220 K and T_{mp} = 309 K.[35] Our data, however, showed no endothermic signal in the temperature range of 300–330 K as shown in Fig. S1 (ESI†), although preparation was attempted many times. Since previous reports also show different results (one reports glass transition and the other shows first-order transition at around 243 K),[34,35] it can be considered that [Li 18C6] has some stable states, and another state was obtained in this study. In the case of [Li 15C5], T_{mp} has only been reported at 356 K.[35] This value was similar to our data; however, we also recorded T_{tr1} at 337 K. In addition, an exothermic peak was detected at 300 K. This signal was also recorded in the first heating run, as displayed in Fig. S1 (ESI†). Because plastic crystals frequently have metastable states and show exothermic peaks during the heating process,[26–33] it can be considered that this exothermic peak corresponds to a phase transition from a metastable state to a stable state. In general, plastic crystals show small $\Delta_{mp}S$ values (< 21 J K^{-1} mol^{-1});[7] however, slightly larger $\Delta_{mp}S$ values were obtained for [Li 15C5], as displayed in Table 1. In contrast, other complexes such as [Li 12C4] and [Na 15C5] showed large $\Delta_{mp}S$ values.

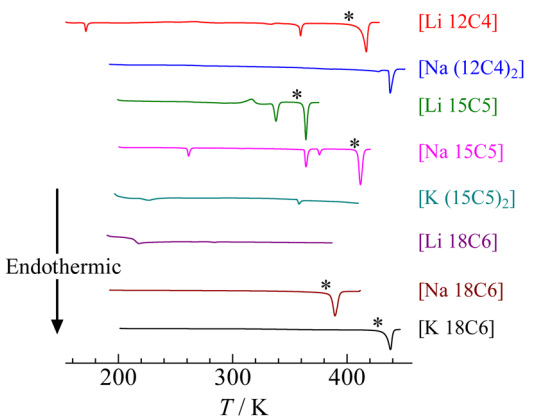

Fig. 2 DSC thermograms of [M (3*n*)C*n*] (M = Li, Na, K.; *n* = 4–6) in the 2nd heating process.

XRD

The powder XRD patterns of the complexes recorded at various temperatures are shown in Fig. 3. The reflection patterns detected in Phase I of [Li 15C5] could be indexed to a cubic structure (a space group of $Pn\bar{3}$) with a lattice constant of a = 1381 ± 5 pm. This result suggests that both the crown ether and the TFSA anion perform isotropic reorientation in the crystal because these molecules have no C3-axis in themselves. Thus, [Li 15C5] could be used as a new ionic plastic crystal. In the case of Phases II and III of [Li 15C5], powder patterns similar to those of Phase I were recorded; therefore, it can be expected that the overall motion of the constituents also occurs in the low-temperature solid phases. In contrast, the powder patterns recorded in Phase I of [Li 12C4] and [Na 15C5] can be fitted by the trigonal structure of $P3$. Lattice constants of a = 928 ± 5, c = 892 ± 5, a = 977 ± 5, and c = 1799 ± 5 were

Table 1 Entropy changes (J mol^{-1} K^{-1}) at each phase transition temperature. The temperatures are shown in parenthesis (K). These values were estimated by the DSC curves of the second heating scan. Decomposition temperatures were determined by TG measurements

	$\Delta_{tr3}S$	$\Delta_{tr2}S$	$\Delta_{tr1}S$	$\Delta_{mp}S$
[Li 12C4]		8.8 ± 0.1 (170 ± 1)	7.3 ± 0.1 (351 ± 1)	31.6 ± 0.1 (400 ± 1)
[Na $(12C4)_2$]			19.5 ± 0.5 (436 ± 1)	Dec. (*ca.* 460)
[Li 15C5]		−11.5 ± 0.5 (300 ± 1)	18.8 ± 0.1 (337 ± 1)	29.2 ± 0.1 (358 ± 1)
[Na 15C5]	7.8 ± 0.1 (358 ± 1)	13.1 ± 0.1 (361 ± 1)	3.6 ± 0.1 (374 ± 1)	35.7 ± 0.5 (405 ± 1)
[K $(15C5)_2$]		1.23 ± 0.01 (219 ± 1)	0.57 ± 0.05 (356 ± 1)	Dec. (*ca.* 440)
[Li 18C6]	The second order transition (213 ± 1)			Dec. (*ca.* 385)
[Na 18C6]				79.4 ± 0.1 (381 ± 1)
[K 18C6]				57.9 ± 0.1 (425 ± 1)

*Dec.: Decomposed.

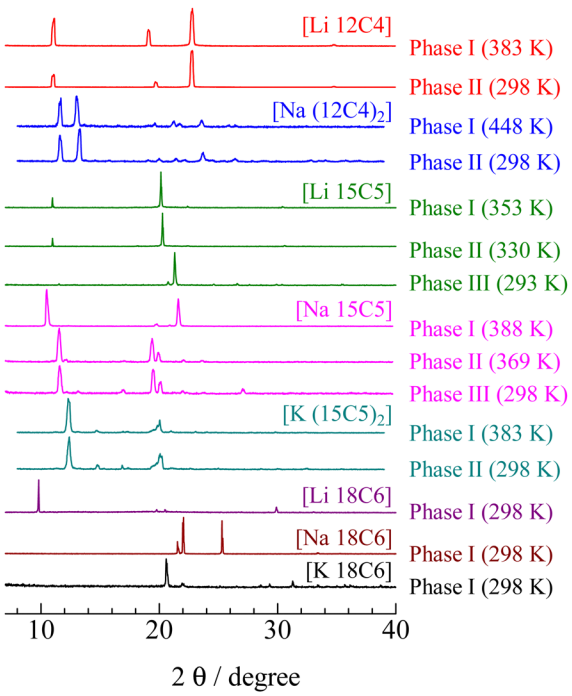

Fig. 3 XRD powder patterns of [M (3*n*)C*n*] (M = Li, Na, K.; *n* = 4–6) observed at each solid phase.

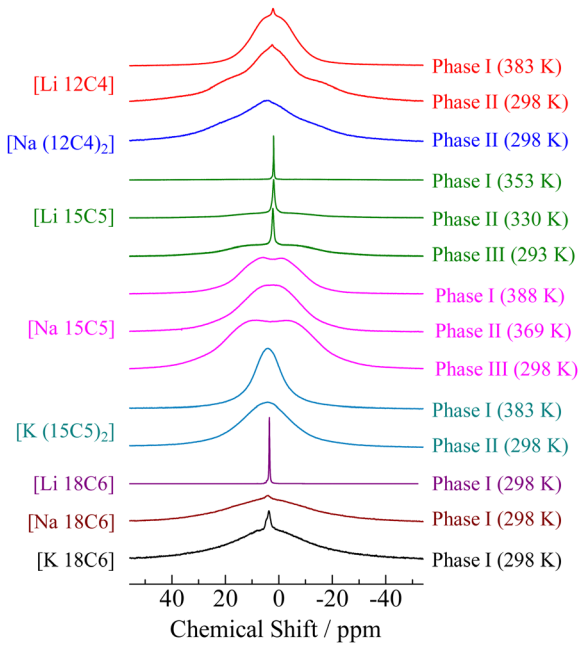

Fig. 4 ^{1}H NMR spectra of [M (3*n*)C*n*] (M = Li, Na, K.; *n* = 4–6) crystals as a function of temperature.

obtained for [Li 12C4] and [Na 15C5], respectively. In the case of the [Li 18C6] crystal, the crystal structure of Phase I could not be uniquely determined. Because the sample showed that the fluidity and the XRD pattern were similar to that observed in liquid crystals, it can be considered that Phase I of [Li 18C6] is a liquid crystalline phase. The other complexes showed complex diffraction patterns, and a unique crystal structure could not be assigned.

^{1}H NMR spectra

Solid-state NMR measurements were performed to assign the motional modes of each compound. The ^{1}H NMR spectra of the complexes are shown in Fig. 4. Narrow line widths are observed, although these signals accumulate without MAS modulation. In general, ^{1}H NMR lines with narrow line widths are difficult to obtain without a high-speed MAS method in ordinal crystals because of the large dipole–dipole interactions among the ^{1}H nuclei. Because Lorentz-type lines with narrow linewidths were detected in Phase I of the [Li 15C5] and [Li 18C6] compounds, it can be considered that the constituents undergo overall motion with large amplitudes (isotropic reorientation). In the case of Phases II and III of [Li 15C5], line envelopes could be fitted by two components: narrow and broad lines, as shown in Fig. S2 (ESI†) and Fig. 4 shows that the amount of the broad component increased in lower-temperature solid phases. Because H atoms are included only in crown ethers, it can be considered that there are two kinds of 15-crown-5 molecules in Phases II and III: one performs isotropic reorientation, similar to the detection in Phase I, and the other undergoes another motion with lower freedom of motion compared with isotropic reorientation. The motion contributing to a broad linewidth is discussed in the following section of ^{13}C NMR. In the case of the [Li 12C4] salt, our ^{1}H NMR spectrum could be separated into two components: one had a narrow linewidth and the

other was broad, as plotted in Fig. S2 (ESI†). Because the NMR spectrum area corresponds to the number of sites, it can be considered that a large amount of crown ether cannot undergo isotropic reorientation in Phase I of [Li 12C4]. This is inconsistent with a previous report in which the [Li 12C4] complex was concluded to be a plastic crystal based on DSC measurements.[34] A more detailed discussion of [Li 12C4] is provided in later sections. For other complexes, broad ^{1}H NMR line envelopes were recorded (Fig. 4). In the case of [Na 15C5], two peaks were detected at *ca.* +8 and −3 ppm in Phase I, although the peak tops of the other samples were obtained at approximately 2 ppm. This result suggests that there are two types of crown ether with different electron densities. This discussion is presented in the following sections. In the case of [Na $(12C4)_2$], our DSC data showed that Phase I was obtained above 436 K. Unfortunately, such high temperatures exceeded the temperature limit of our NMR apparatus; therefore, no spectrum was observed for Phase I of [Na $(12C4)_2$].

Molecular motion in crystals is often linked to the M_2 values of the ^{1}H NMR absorption lines. The $M_{2\,\mathrm{Obs}}$ values were estimated using the following relationship:36,37

$$M_{2\,\mathrm{Obs}} = \langle \omega^2 \rangle = \frac{\int (\omega_0 - \omega)^2 f(\omega_0 - \omega) \mathrm{d}\omega}{\int f(\omega_0 - \omega) \mathrm{d}\omega} \quad (1)$$

Here, ω_0 and $f(\omega_0 - \omega)$ are the angular frequency (rad s^{-1}) of the peak top and line height at $\omega_0 - \omega$, respectively. We analysed the lines using Lorentz functions, as displayed in Fig. S2 (ESI†) in which some data are displayed. The $M_{2\,\mathrm{Obs}}$ values estimated from each analysed line are summarised in Table 2. The theoretical $M_{2\,\mathrm{Cal}}$ values can be estimated using the following relationship:[36,37]

$$M_{2\,\mathrm{Cal}} = \frac{3\gamma_I^4 \hbar^2 I(I+1)}{4N} \sum_{i,j} \frac{\left(1 - 3\cos^2\theta_{ij}\right)^2}{r_{ij}^6} + \frac{\gamma_I^2 \gamma_S^4 \hbar^2 S(S+1)}{3N} \sum_{i,k} \frac{\left(1 - 3\cos^2\theta_{ik}\right)^2}{r_{ik}^6} \quad (2)$$

Here, γ_I, γ_S, I, S, N, h, θ, and r are the gyromagnetic ratios of nuclei I (^{1}H) and S (^{7}Li, ^{23}Na, *etc.*), nuclear spin quantum number of ^{1}H (I = 1/2) and S, number of nuclei counted in the calculation, Plank's constant, angle between the static magnetic field and *I*–*I* and *I*–*S* vectors, and length of *I*–*I* and *I*–*S* vectors, respectively. In this study, the $M_{2\,\mathrm{Cal}}$ values were estimated for one cation; only intramolecular interactions were calculated (in the case of $[\mathrm{Na}\ (12C4)_2]^+$ and $[\mathrm{K}\ (15C5)_2]^+$, sandwich structures reported in previous studies[44] are assumed). The results are summarised in Table 3. In this table, each $M_{2\,\mathrm{Cal}}$ value with M ions is similar to that without M ions. This result can be explained by the effects of small γ_S values of Li, Na, and K, and large M–H distances compared with those between H and H separations. Our $M_{2\,\mathrm{Cal}}$ values were similar to those reported for 15-crown-5 and 18-crown-6.[42] Because the contributions of intermolecular interactions can be roughly estimated to be approximately 0.5–1.5 G^2, the observed M_2 value of 0.12 G^2 in the Phase I of [Li 15C5] can be assigned to isotropic reorientation. The $M_{2\,\mathrm{Obs}}$ value of <1.5 G^2 is also assigned to isotropic reorientation, and the ^{1}H NMR lines recorded in the Phase I of [Li 18C6] and the narrow component in Phases II and III of [Li 15C5] and in Phase I of [Na 18C6] and [K 18C6] can be assigned to the isotropic reorientation of the crown ether molecule. In contrast, it can be attributed to the Phase I of [Li 12C4], Phases I and II of [Na 15C5], and Phase I of $[\mathrm{K}\ (15C5)_2]$ being rotator phases, as compared with the $M_{2\,\mathrm{Obs}}$ and $M_{2\,\mathrm{Calc}}$ values of uniaxial rotation.

Because the relationship $M_{2\,\mathrm{Obs}} < 1$ is often obtained in plastic crystals, it can be expected that the constituents undergo self-diffusion in Phase I of [Li 15C5] and [Li 18C6] in addition to isotropic rotational motion. In the lower-temperature phases of

Table 2 Values of the full width $\Delta\nu$ (kHz) at half-maximum and the second moments $M_{2\,\mathrm{Obs}}$ (G^2). These values were determined by analysing the ^{1}H NMR lines

	Phase	$\Delta\nu$/kHz	$M_{2\,\mathrm{Obs}}/G^2$	
[Li 12C4]	I	0.60 ± 0.01	0.39 ± 0.01	Isotropic rotation
		11.2 ± 0.5	4.66 ± 0.05	Uniaxial rotation
	II	6.8 ± 0.5	4.12 ± 0.05	Uniaxial rotation
		28.8 ± 0.5	8.05 ± 0.05	
$[\mathrm{Na}\ (12C4)_2]$	II	16.6 ± 0.5	8.93 ± 0.05	
[Li 15C5]	I	0.18 ± 0.01	0.12 ± 0.01	Isotropic rotation
	II	0.49 ± 0.01	0.32 ± 0.01	Isotropic rotation
		17.5 ± 0.5	9.3 ± 0.05	
	III	0.55 ± 0.01	0.36 ± 0.01	Isotropic rotation
		23.8 ± 0.5	11.7 ± 0.5	
[Na 15C5]	I	9.4 ± 0.5	5.51 ± 0.05	Uniaxial rotation
		8.8 ± 0.5	5.20 ± 0.05	Uniaxial rotation
	II	10.3 ± 0.5	5.97 ± 0.05	Uniaxial rotation
		10.3 ± 0.5	5.97 ± 0.05	Uniaxial rotation
	III	13.3 ± 0.5	7.46 ± 0.05	
		13.3 ± 0.5	7.48 ± 0.05	
$[\mathrm{K}\ (15C5)_2]$	I	7.2 ± 0.5	4.34 ± 0.05	Uniaxial rotation
	II	13.5 ± 0.5	7.53 ± 0.05	
[Li 18C6]	I	0.18 ± 0.01	0.12 ± 0.01	Isotropic rotation
[Na 18C6]	I	1.90 ± 0.05	1.22 ± 0.05	Isotropic rotation
		23.9 ± 0.5	11.7 ± 0.05	
[K 18C6]	I	0.90 ± 0.05	0.59 ± 0.01	Isotropic rotation
		19.7 ± 0.5	10.2 ± 0.5	

Table 3 Theoretical $M_{2\,\mathrm{Cal}}$ values in G^2. The values were estimated for one cation (only the intramolecular interaction was calculated)

	Models	$[\mathrm{M\ 18C6}]^+$	$[\mathrm{M\ 15C5}]^+$	$[\mathrm{M\ 12C4}]^+$
Without alkali metal ions	Rigid	15.05	16.53	15.70
	Uniaxial rotation	1.46	4.06	5.62
	Isotropic rotation	0.00	0.00	0.00
Li	Rigid	15.05	16.53	15.70
	Uniaxial rotation	1.49	4.12	5.65
	Isotropic rotation	0.00	0.00	0.00
Na	Rigid	15.05	16.53	18.13[a]
	Uniaxial rotation	1.47	4.09	7.77[a]
	Isotropic rotation	0.00	0.00	0.00
K	Rigid	15.05	17.42[b]	
	Uniaxial rotation	1.46	4.36[b]	
	Isotropic rotation	0.00	0.00	

[a] $[\mathrm{Na}\ (12C4)_2]^+$. [b] $[\mathrm{K}\ (15C5)_2]^+$.

[Li 15C5], the narrow components of $M_{2\,\mathrm{Obs}}$ = 0.32 (Phase II) and 0.36 G^2 (Phase III) can also be assigned to diffusion. In contrast, the broad components of 9.3 and 11.7 G^2 could hardly be linked to isotropic reorientation. Based on these results, it can be illustrated that a few crown ethers can perform isotropic reorientation; however, most molecules perform motions with smaller degrees of freedom compared with isotropic reorientation in Phases II and III of [Li 15C5]. This model is consistent with our conductivity data, as described in the later section (the [Li 15C5] crystal showed large conductivity). In the case of Phase I of [Li 12C4] which was reported to be in the plastic crystalline phase,[34] one component with an $M_{2\,\mathrm{Obs}}$ value of 0.39 G^2 can be linked to isotropic reorientation and diffusion (the [Li 12C4] crystal also showed high conductivity). However, the main component with an $M_{2\,\mathrm{Obs}}$ value of 4.66 G^2 cannot be attributed to isotropic reorientation.

^{13}C NMR spectra

The ^{1}H NMR spectra provide information about the averaging of the dipole–dipole interactions by molecular motion. In contrast, the line shapes of the ^{13}C NMR spectra were mainly determined by CSA because the magnetic dipole moments of the ^{1}H nuclei were decoupled in this measurement. The ^{13}C NMR spectra observed for the crystals of [M (3*n*)C*n*] (M = Li, Na, K. *n* = 4–6) are shown in Fig. 5. If the ^{13}C NMR spectra were observed in solution, two peaks could be detected: one was assigned to the crown ethers (~70 ppm) and the other was linked to the anion (~120 ppm). In our apparatus, the dipole moments of ^{19}F nuclei could not be decoupled. Therefore, it can be expected that signals assigned to the anion show a large linewidth unless the anion undergoes motions with a large degree of freedom of motion, for example, isotropic reorientation. In the case of Phase I of [Li 15C5] and [Li 18C6], the quartet signals attributed to spin coupling with ^{19}F (I = 1/2) were detected at approximately 120 ppm, in addition to the narrow lines without CSA at approximately 70 ppm. Based on these results, it can be concluded that both crown ether molecules and anions exhibit isotropic reorientation in Phase I of the [Li 15C5] and [Li 18C6] complexes. This result is consistent with the ^{1}H NMR spectra. In the case of Phase I of [Li 12C4], a line envelope with CSA was recorded at approximately 70 ppm. In addition, a broad peak was recorded at approximately 120 ppm. These results also support that [Li 12C4] should not be classified as a plastic crystal, although the previous paper reported that [Li 12C4] is a plastic crystal.[34] The line shape detected at *ca.* 70 ppm could be fitted by powder patterns of axial-symmetric CSA ($\sigma_{xx} = \sigma_{yy} \neq \sigma_{zz}$) rather than static-type line envelopes ($\sigma_{xx} \neq \sigma_{yy} \neq \sigma_{zz}$) as demonstrated in Fig. S3 (ESI†); therefore, it can be regarded that the 12-crown-4 molecule performs a uniaxial motion in Phase I. This assignment is consistent with our results (an $M_{2\,\mathrm{Obs}}$ value of 4.66 G^2 and a *P*3 crystal structure). In the ^{1}H NMR spectrum, the sharp component can be assigned to isotropic reorientation; however, the ^{13}C NMR line shape can be fitted without its component. Because the amount of the component is small, as described above, it can be considered that its contribution to the ^{13}C NMR spectrum is small. In Phase II, the spectrum can be fitted by two components: an axial-symmetric CSA and a static-type line envelope. This result is consistent with the M_2 results. The estimated CSA values are presented in Table 4. Based on these results, it can be concluded that the [Li 12C4] complex was a rotator crystal rather than a plastic crystal. This determination was also supported by our ^{7}Li NMR spectra, as discussed in the next section.

In Phases II and III of [Li 15C5], the ^{13}C NMR signals recorded at approximately 70 ppm could be fitted by two components, as shown in Fig. S3 (ESI†). One is a Lorentz-type adsorption line and the other is a CSA-type function. This result

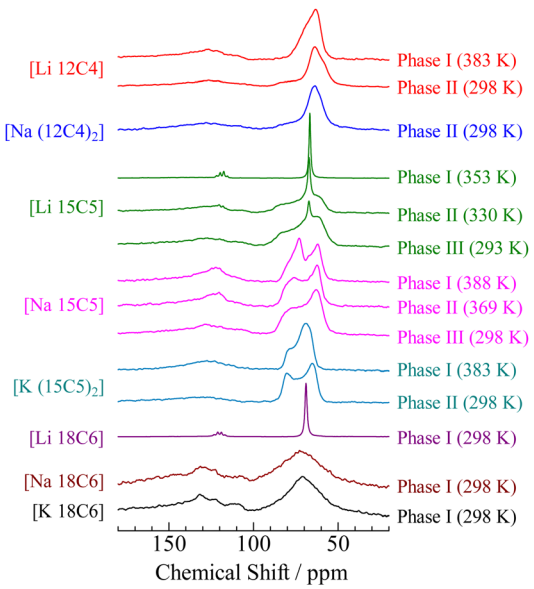

Fig. 5 ^{13}C NMR spectra of [M (3*n*)C*n*] (M = Li, Na, K.; *n* = 4–6) crystals as a function of temperature.

Table 4 Estimated chemical shift values (σ_{zz}, σ_{yy}, and σ_{xx}) in ppm. These values were obtained from analysed lines as displayed in Fig. S3 (ESI)

	Phase	σ_{zz}	σ_{yy}	σ_{xx}
[Li 12C4]	I	76 ± 1	61 ± 1	—
	II	86 ± 1	63 ± 1	—
		68 ± 1	60 ± 1	55 ± 1
[Na (12C4)$_2$]	II	86 ± 1	64 ± 1	63 ± 1
		69 ± 1	62 ± 1	58 ± 1
[Li 15C5]	I	66.7 ± 0.5	—	—
	II	67.1 ± 0.5	—	—
		87 ± 1	64 ± 1	58 ± 1
	III	67.2 ± 0.5	—	—
		87 ± 1	63 ± 1	56 ± 1
[Na 15C5]	I	79 ± 1	73 ± 1	71 ± 1
		70 ± 1	62 ± 1	60 ± 1
	II	84 ± 2	76 ± 2	69 ± 2
		71 ± 2	62 ± 2	60 ± 2
	III	86 ± 2	77 ± 2	71 ± 2
		72 ± 2	63 ± 2	58 ± 2
[K (15C5)$_2$]	I	81 ± 2	79 ± 2	73 ± 2
	II	74 ± 2	69 ± 2	64 ± 2
[Li 18C6]	I	69.9 ± 0.5	—	—
[Na 18C6]	I	89 ± 4	72 ± 4	56 ± 4
[K 18C6]	I	82 ± 3	71 ± 3	56 ± 3

is consistent with the ^{1}H NMR spectra displayed in Fig. 3, where the two components form the ^{1}H NMR line envelope. At *ca.* 120 ppm, a quartet signal was detected in phases II and III. The intensity decreased from Phase I, and the component with a narrow linewidth recorded at ~70 ppm was also reduced. Based on these results, the number of cations and anions performing isotropic reorientation was reduced in the lower-temperature phase. This tendency is also consistent with the ^{1}H NMR spectra.

In the case of [Na 18C6] and [K 18C6], broad signals were recorded at around 70 and 120 ppm, respectively; therefore, it can be concluded that these compounds form ordinal crystals in each highest-temperature solid phase. This conclusion is consistent with the ^{1}H NMR and XRD results. Unfortunately, we could not observe any NMR spectrum of Phase I of [Na $(12C4)_2$] because of the limited temperature of our apparatus. In the case of [Na 15C5], two signals were recorded at approximately 62 and 73 ppm. This difference was also detected in 18-crown-6–KSCN complexes.[41] Buchanan explained that there are two different conformational structures of the crown ether ring in the crystal; therefore, we prepared a single crystal of [Na 15C5] and single crystal XRD (SCXRD) measurements were conducted. The results are described in the following section on SCXRD.

^{7}Li NMR spectra

Since the nuclear spin quantum number of ^{7}Li is 3/2, quadrupole effects contributing to ^{7}Li NMR spectra are generally observed, and the spectra show satellite peaks beside the central signal if the nucleus experiences the anisotropic charge distribution spatially.[38] The separation between the satellites (Δ in Hz) depends on the QCC values. If both the Li–crown-ether cation and the TFSA anion undergo isotropic reorientation, a Lorentz-type function accompanied with no satellite peaks is detected in the ^{7}Li NMR spectrum. The results obtained for [Li 12C4], [Li 15C5], and [Li 18C6] are shown in Fig. 6. A signal with half-height full linewidths ($\Delta\nu$) of 1.4 and 1.1 kHz was recorded in Phase I of [Li 15C5] and [Li 18C6], respectively. Because no signal was accompanied by satellite peaks, it can be regarded that the constituents perform isotropic reorientation. This result is consistent with the ^{1}H and ^{13}C NMR data. In contrast, the $\Delta\nu$ value of 4.2 kHz was recorded in Phase I of [Li 12C4]. In this phase, the ^{1}H and ^{13}C NMR spectra showed that the crown ether molecules underwent uniaxial rotation rather than isotropic reorientation. Therefore, it can be assumed that the linewidth includes the satellite peaks. This assumption yields a QCC value of 8.4 kHz. In Phase II of [Li 12C4], the satellite signals could be fitted by the typical line shape of a first-order quadrupolar interaction with nonzero asymmetry parameters (η). The analysed lines of the satellite signals are also plotted in Fig. 6. The estimated QCC value of 22.4 kHz was significantly smaller than that of 60–68 kHz reported in the 12-crown-4–LiCl complex.[40] In previous studies, it was reported that the Li ion undergoes an anisotropic vibration in the crown ether, and the motion causes larger QCC values. In this study, η = 0.40 could be estimated in Phase II. This value indicates the presence of crown ether molecules without a uniaxial rotation. The ^{1}H and ^{13}C NMR spectra were fitted by two components, as shown in Fig. 4 and 5, respectively. Based on these facts, it can be concluded that each broad component recorded in the ^{1}H and ^{13}C NMR spectra is related to ^{7}Li satellite peaks. In the case of Phase II and III of [Li 15C5], satellite signals were recorded as shown in Fig. 6. This result is consistent with the ^{1}H and ^{13}C NMR data. Since the line shapes were complex, the line envelope could not be fitted by unique functions.

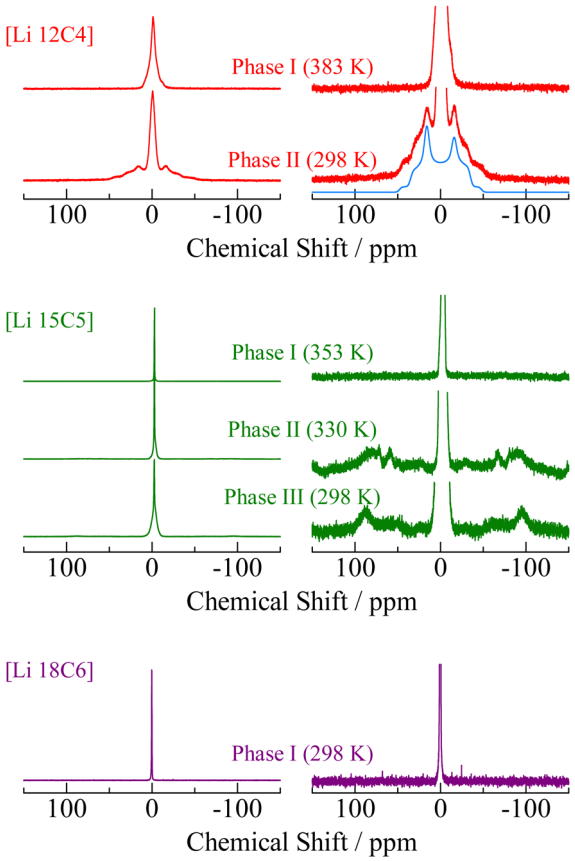

Fig. 6 ^{7}Li NMR spectra of [Li $(3n)$Cn] (n = 4–6) crystals as a function of temperature. Expanded signals are displayed at the right side. The blue solid line is analysing curves.

^{1}H NMR relaxation times

To obtain information about ionic motion, relaxation time measurements were performed. An inversion recovery method was applied to estimate the ^{1}H NMR T_1. In this method, the magnetic recovery curves can be fitted using the following function:[37,38]

$$L(\tau) = \ln\frac{M^{eq} - M(\tau)}{2M^{eq}} = -\frac{\tau}{T_1} \quad (3)$$

Here, M^{eq} and $M(\tau)$ are the magnitudes of the magnetisations along the static magnetic field at thermal equilibrium and at an interval of τ, respectively. The magnetic recovery curve is shown in Fig. 7. Using eqn (3), a T_1 value could be determined

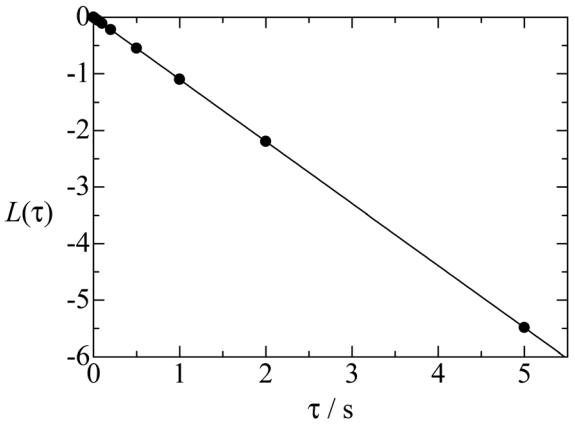

Fig. 7 Magnetic recovery curve of [Li 12C4] at 318 K.

from the slope of the recovery curve. The recovery curves obtained at each temperature for each complex could be fitted by one component; therefore, one type of motion (isotropic reorientation, uniaxial rotation, *etc.*) mainly contributes to the relaxation process of ^{1}H nuclear spins. The temperature dependence of ^{1}H NMR T_1 values obtained for each complex is plotted in Fig. 8. For [Li 15C5], the T_1 values increased with increasing temperature in the plastic phase (Phase I). This tendency is similar to that reported for [NR_4][BEt_3R']-type plastic crystals.[26–30] In contrast to Phase I, a T_1 minimum was obtained in Phase II. If the ^{1}H relaxation process is caused by the fluctuation of dipole–dipole interactions between spins, the T_1 values can be described by the following relationship:[37]

$$\frac{1}{T_1} = \frac{2\tau_c \Delta M_2}{3}\left(\frac{\tau_c}{1+\omega_0^2\tau_c^2} + \frac{4\tau_c}{1+4\omega_0^2\tau_c^2}\right) \quad (4)$$

where τ_c and ω_0 are the correlation time and observed angle frequency ($2\pi \times 600.13$ MHz in this study), respectively. Based on this equation, a T_1 minimum is recorded if $\tau_c \sim \omega_0$. In addition, the relationship indicates that T_1 is inversely proportional to τ_c if $\tau_c \ll \omega_0$. In general, τ_c can be linked to the Arrhenius relationship:[37]

$$\tau_c = \tau_0 \exp\left(\frac{E_a}{RT}\right) \quad (5)$$

where τ_0 is the correlation time at $T = \infty$. Eqn (4) shows the following relationship at the temperature of T_1 minimum:

$$T_1 \sim \frac{\omega_0}{\Delta M_2} \quad (6)$$

Substituting the T_1 minimum value of 660 ms into eqn (6) and (2), the r value of approximately 250 pm was estimated. This value corresponds to the H–H distance between neighbouring CH_2 groups; therefore, it can be considered that the T_1 relaxation detected in Phase II of [Li 15C5] is caused by isotropic reorientation. This assignment is supported by the fact that the T_1 relaxation speed in Phase I was slightly higher owing to the phase transition at T_{tr1}. Using eqn (4) and (5), E_a values of 25 ± 1 and 34 ± 1 kJ mol^{-1} were estimated for the isotropic reorientation motion in Phase I and Phase II of

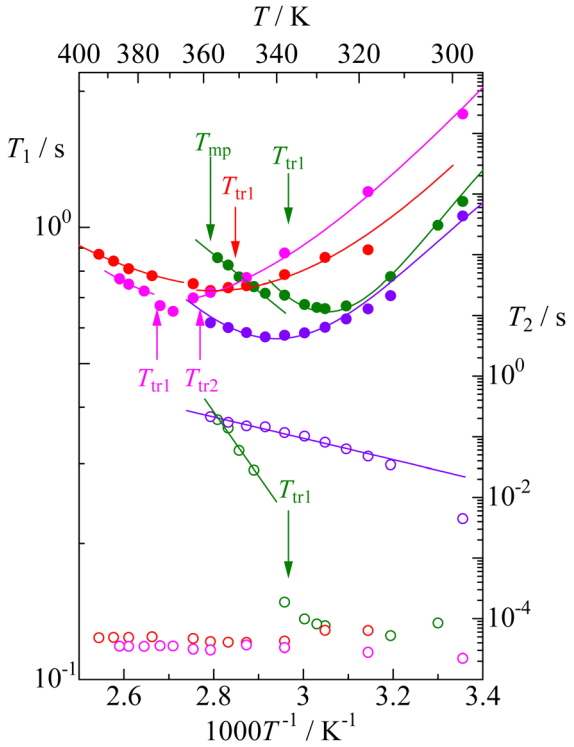

Fig. 8 Temperature dependences of ^{1}H NMR T_1 and T_2 obtained in [Li 12C4] (● and ○), [Li 15C5] (● and ○), [Li 18C6] (● and ○), and [Na 15C5] (● and ○), respectively.

[Li 15C5], respectively. In the case of [Li 18C6], the E_a value of 26 ± 1 kJ mol^{-1} was obtained. These values are larger than those reported for [NR_4][BEt_3R'] (R, R′ = Me, Et)-type plastic crystals.[26–30] This difference from [NR_4][BEt_3R'] can be explained by the size of the constituents. For the other samples, the T_1 slopes gave E_a values as listed in Table 5. Since T_1 minima were recorded in Phase II of [Li 15C5] and Phase I of [Li18C6], τ_0 values of 6.2×10^{-14} s and 2.1×10^{-14} s were also estimated using eqn (4) and (5), respectively.

To estimate the E_a values of the ion jump, ^{1}H NMR T_2 was used. The spin echo method was applied at each temperature. The results are also shown in Fig. 8. T_2 relaxation is a function of the correlation time of the self-diffusion motion, and its value can be described by the following relationships:[39]

$$\frac{1}{T_2} \propto M_2\tau_c = M_2\tau_0 \exp\left(\frac{E_a}{RT}\right)\left(\tau_C\sqrt{M_2} \ll 1\right) \quad (7)$$

Table 5 Activation energies E_a in kJ mol^{-1} and corresponding motional modes in each phase of the salts. In this table, the accuracy is 1 kJ mol^{-1}. These values are estimated by T_1 data

	Phase I	Phase II	Phase III
[Li 12C4]	17 (Uniaxial)	21 (Uniaxial)	
[Li 15C5]	25 (Isotropic)	34 (Uniaxial)	
[Na 15C5]	22 (Uniaxial)	DA	21 (Uniaxial)
[Li 18C6]	26 (Isotropic)		

Isotropic: isotropic reorientation, Uniaxial: uniaxial rotation, DA: difficult of analysing.

$$\frac{1}{T_2} \propto \sqrt{M_2}\left(\tau_C\sqrt{M_2} \gg 1\right) \quad (8)$$

These relationships indicate that T_2 increases with temperature ($\tau_C\sqrt{M_2} \ll 1$) and is independent of temperature ($\tau_C\sqrt{M_2} \gg 1$). In Phase I of [Li 15C5] and [Li 18C6], the T_2 increment was obtained; therefore, it can be regarded that the crown ether molecules undergo self-diffusion in each crystal. Using eqn (7), E_a values of 202 ± 1 and 34 ± 3 kJ mol^{-1} were estimated for Phase I of [Li 15C5] and [Li 18C6], respectively. The large difference between these complexes can be explained by the fluidity of the [Li 18C6] compound. For [Li 12C4] and [Na 15C5] and Phase II of [Li 15C5], T_2 values were independent of temperature. This suggests that the correlation times of the self-diffusion of the molecules are long compared with those in Phase I of [Li 15C5].

SCXRD

The ^{1}H and ^{13}C NMR spectra of [Na 15C5] show two peaks as shown in Fig. 4 and 5, respectively. This result indicates that crown ether molecules have two types of environments in the crystal. To reveal this fact, a single crystal of the [Na 15C5] complex was prepared using a slow evaporation method using diethyl ether, and the SCXRD analysis was performed. The obtained crystals were well-formed, colourless, block-shaped crystals. SCXRD studies revealed that in crystal packing, the molecules form a 2D tape *via* short and weak interactions C–H···O (3.538 Å, 155.02°), C–H···N (3.599 Å, 144.56°), and C–H···O (3.37 Å, 129.01°) along the *bc* plane in a monoclinic crystal system with the space group $C2/c$ with Z = 8 at 293 K (Fig. S4, ESI†). However, the crown ether rings exhibited conformational disorder even at a low temperature of 253 K (Fig. 9), with the labile attachment of crown ether and Na^+. The weak intermolecular interactions can favour spatially loose crystal packing, allowing increased molecular movements, resulting in conformational disorder in the crown ether ring. SCXRD measurements revealed that the occupancy of one state was slightly larger than that of the other, and the ratio difference in occupancy decreased with the increasing temperature (28 : 72 at 253 K was changed to 32 : 68 at room temperature). Based on our analysis, it can be concluded that the crown ether molecule jumps between two stable states, rather than two exact sites in the crystal. Since we obtained rare results (^{1}H and ^{13}C NMR spectra showed two signals), the detailed discussion will present in another paper.

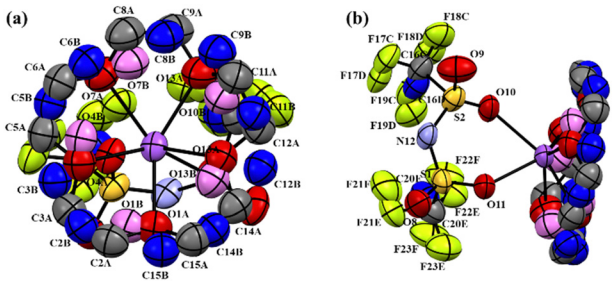

Fig. 9 ORTEP representation of [Na 15C5] at 253 K temperature where the disordered parts A and B occupancy were 72% and 28%, respectively. The low occupancy part of the disordered molecules carbon, oxygen and fluorine are coloured as blue, violet and green, respectively. Hydrogens are omitted for clarity.

Electrical conductivity

To detect the translational motion of ions, electrical conductivity measurements were performed as a function of temperature. The results are plotted in Fig. S5 (ESI†). The obtained σ values of [Li 12C4] reaching 6.85 × 10^{-4} S cm^{-1} are similar to those reported in the literature.34 In the case of [Li 15C5], the σ value rapidly increased with the increasing temperature and reached 2.52 × 10^{-4} S cm^{-1}. This value is similar to those of some Li compounds.[16–22,46–52] A σ jump was detected at a T_{tr1} of 337 K. Discontinuities were also recorded at the T_{tr} of some complexes. This phenomenon is often observed in first-order phase transitions. In the case of [Li 18C6], the crystal was very soft; therefore, we could not make any pellets. In [K 18C6], the σ values could not be recorded because of the high resistance values. Phase I of [Na $(12C4)_2$] and Phase III of [Li 15C5] were outside the temperature ranges of our apparatus; therefore, no σ values could be obtained.

The function ln (σT) can be described by the following relationship:

$$\ln(\sigma T) \propto -\frac{E_{a\,diff}}{RT} \quad (9)$$

Plotting ln(σT) as a function of T^{-1} (Fig. 10), the activation energies ($E_{a\,diff}$) listed in Table 6 were obtained. For [Li 15C5] and [Na 18C6], σ values rapidly increased just below the melting temperature. Therefore, we estimated $E_{a\,diff}$ values in the high- and low-temperature ranges of Phase I. Activation energies of 620 and 127 kJ mol^{-1} were obtained in the high- and low-temperature ranges of the plastic phase of [Li 15C5], respectively. The former value is much larger than 202 kJ mol^{-1} estimated by the ^{1}H T_2

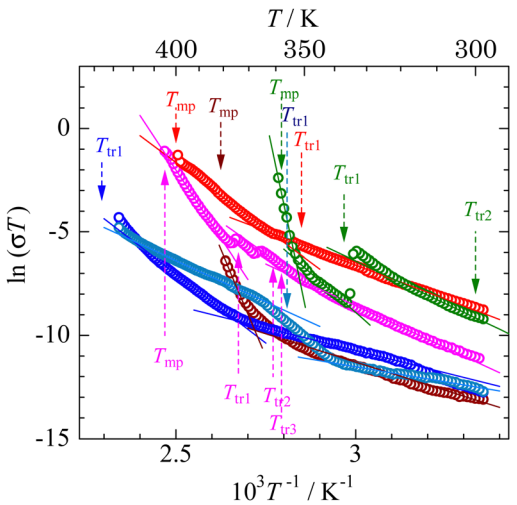

Fig. 10 Arrhenius plots of electrical conductivity. [Li 12C4] (○), [Na $(12C4)_2$] (○), [Li 15C5] (○), [Na 15C5] (○), [K $(15C5)_2$] (○), and [Na 18C6] (○).

Table 6 Activation energies $E_{a\,diff}$ in kJ mol^{-1} estimated by conductivity measurements

	Phase I	Phase II	Phase III
[Li 12C4]	107 ± 10	55 ± 5	—
[Na (12C4)$_2$]	—	111 ± 10, 36 ± 5[a]	
[Li 15C5]	620 ± 50[b], 127 ± 10	68 ± 5	—
[Na 15C5]	220 ± 10	103 ± 10	67 ± 5
[K (15C5)$_2$]	66 ± 5	24 ± 3	
[Na 18C6]	340 ± 10[b], 46 ± 5		

[a] Value in the low temperature range of Phase II. [b] Value in the high temperature range of Phase I.

measurement; in contrast, the latter is small. Conductivity measurements detect the self-diffusion of ions (the crown ether molecule motion can rarely be estimated); in contrast, the motion of crown ether molecules contributes to ^{1}H NMR T_2 values. As described in the previous section, the effects of the Li magnetic moment on the M_2 values are little. Because T_2 is related to M_2 as shown in eqn (7), it can be considered that the effects of the motion of Li ions on the ^{1}H T_2 relaxation process are negligible. The ^{13}C NMR spectrum recorded in Phase II of [Li 15C5] showed that the anion rarely underwent isotropic reorientation, as displayed in Fig. 5. In contrast, the intensity of the satellite peaks of the ^{7}Li NMR signal was lower than that of [Li 12C4], as shown in Fig. 8. Based on these results, it can be concluded that the $E_{a\,diff}$ values of 620 and 127 kJ mol^{-1} are the translational motions of the TFSA anion and Li cation, respectively.

Experimental

Sample preparation

Because the products showed hygroscopicity, all treatments were performed in a glove box in which air was completely substituted by N_2 gas. 2.5 mmol of crown ethers of [12C4], [15C5], and [18C6] (Tokyo Kasei) and Li-TFSA (Tokyo Kasei) were mixed in 20 mL of dichloromethane solvent (Kantou Kagaku). In the case of [Na (12C4)$_2$] and [K (15C5)$_2$] preparation, 5.0 mmol of [12C4] and [15C5] were added to the same volume of the solvent with the same amount (2.5 mmol) of Na-TFSA (Kantou Kagaku) and K-TFSA (Wako Jyunyaku), respectively. In the other samples of [Na 15C5], [Na 18C6], and [K 18C6], the same amounts of crown ethers and M-TFSA were mixed in the same volume of the solvent. The mixed solution was stirred at room temperature for 24 h. After filtering the residue from each solution, the solutions were evaporated at 80 °C. The solids were then washed with a large amount of diethyl ether (Kantou Kagaku). The crystals were dried under vacuum.

Measurements

Differential scanning calorimetry (DSC) measurements were performed using a Hitachi Hightech DSC-7020 calorimeter. All samples were placed in aluminium pans (h = 5 mm and ϕs. Heating and cooling rates of 10 K min^{-1} were employed. In this study, some compounds were decomposed by heating; therefore, a thermogravimetric (TG) analysis was performed using a Hitachi Hightech STA7300 calorimeter.

XRD powder patterns were recorded using a Bruker D8 ADVANCE diffractometer equipped with a Cu anticathode. A TTK450 probe was employed at various temperatures. The powder patterns were plotted in the scan range of 6–40° with an angular step size of 0.02°. Single-crystal X-ray diffraction (SCXRD) data of [Na 15C5] were collected using a Bruker D8 VENTURE (PHOTON III 14) and a nitrogen-flow temperature controller using graphite monochromated Mo-Kα radiation (λ = 0.71073 Å) at 293 and 253 K. Intrinsic phasing methods (SHELXT)[53] were used to solve the structure, and full-matrix least-squares calculations on F^2 (SHELXL)[54,55] were used to refine the structure. The non-hydrogen atoms were refined anisotropically. Mercury CSD was used to measure the distances and angles in the structural analysis.

Solid-state ^{1}H, ^{7}Li, and ^{13}C NMR spectra were recorded at Larmor frequencies of 600.13, 233.23, and 150.92 MHz, respectively, using a Bruker Avance 600 spectrometer (14.10 T). The samples were sealed in handmade glass tubes with an outer diameter of approximately 4 mm. The spectra were obtained by Fourier transform (FT) of the free induction decay (FID) signals recorded after π/2 (^{1}H and ^{13}C) and π/4 (^{7}Li) pulses with recycling times of 5 s (^{1}H and ^{7}Li) and 20 s (^{13}C). The ^{1}H, ^{7}Li, and ^{13}C NMR chemical shifts were calibrated relative to the external references of water (δ = 4.80 ppm), LiCl aqueous solution of 1 mol dm^{-3} (δ = 0 ppm) and glycine (δ = 43.16 ppm), respectively. Glycine signals were observed with an MAS rate of 5 kHz, using the cross-polarisation (CP) method. T_1 and T_2 values were obtained by inversion recovery (pulse sequence: π–τ–π/2) and spin-echo (π/2–τ–π–τ) methods, respectively. The sample temperature was controlled using a Bruker VT-3000 instrument. The whole data accumulation started after 10 min of waiting at each temperature.

Electrical conductivity measurements at 1 kHz were performed at temperatures ranging from 298 K to just below each melting point using a two-terminal method employing an Agilent Technologies E4980A Precision LCR meter equipped with an Al sheet. The powdered sample was pressed into a disc with a diameter of 1 cm and a thickness of approximately 1 mm at 20 kPa. Because the specimens were hygroscopic, the air around the probe was replaced with dry N_2 gas.

To analyse the NMR data, density functional theory (DFT) simulations were performed using the Gaussian 16 computer program. We used a B3LYP/6-311 + G** function for the estimation of shielding tensors because it is in agreement with the experimental ^{13}C NMR peaks and linewidths of alkylammonium and alkylboronate ions.[26–28] The atomic coordinates of each cation and anion were optimised using the B3LYP/6-311 + G**function. The calculated CS values were determined by the difference in the shielding tensor estimated in a tetramethyl silane (TMS) molecule, and the same function was applied to optimise the atomic coordinates and estimate the shielding tensor of TMS.

Conclusions

This study provides the first evidence that Li ions can form ionic plastic crystals using crown ether with TFSA. The ^{1}H, ^{7}Li,

and ^{13}C NMR spectra showed that the constituents underwent isotropic reorientation in the plastic crystalline phase (337–358 K) of [Li 15C5]. ^{1}H NMR T_1 measurements also revealed that the activation energy of the motion was 25 kJ mol^{-1}. This value is larger than that reported for [NR_4][BEt_3R'] (R, R′ = Me, Et)-type plastic crystals.[26–30] This difference could be explained by the sizes of the constituents. The [Li 15C5] crystal had a cubic structure in Phase I and a small $\Delta_{mp}S$ value of 29.2 J mol^{-1} K^{-1}. The temperature dependences of the ^{1}H NMR T_2 values and electrical conductivity indicated that the 15-crown-5 molecule underwent self-diffusion with an $E_{a\,diff}$ value of 202 kJ mol^{-1}, and the Li ion and the counter ion underwent translational motion with $E_{a\,diff}$ values of 127 and 620 kJ mol^{-1}, respectively.

In Phase I of the [Li 18C6] complex, our ^{1}H, ^{7}Li, and ^{13}C NMR measurements revealed that the constituents underwent isotropic reorientation. However, this complex exhibited fluidity. In addition, the XRD patterns could not be indexed to any cubic structure, and the pattern was similar to that of the liquid crystal. Based on these facts, we conclude that the complex cannot be classified as a plastic crystal. The ^{1}H NMR T_1 and T_2 observations revealed that the 18-crown-6 molecule exhibited isotropic reorientation and self-diffusion with E_a values of 26 and 34 kJ mol^{-1}, respectively.

[Li 12C4] has been reported to be a plastic crystal, based on DSC measurements.[34] However, ^{1}H, ^{7}Li, and ^{13}C NMR spectra revealed that the 12-crown-4 molecule underwent uniaxial rotation in the highest-temperature solid phase. Thus, we conclude that this complex is a rotator crystal rather than a plastic crystal. The crystal had high σ values reaching 6.85 × 10^{-4} S cm^{-1} in Phase I. This value is similar to that reported in the literature.[34]

We also treated Na and K complexes. Based on the results of the ^{1}H and ^{13}C NMR spectra, it can be considered that the [Na 15C5] and [K $(15C5)_2$] compounds are new rotator crystals. In the former complex, SCXRD measurements revealed that 15-crown-5 had two stable sites in the crystal.

Author contributions

A. K.: investigation, formal analysis, and methodology; J. Y: investigation, formal analysis, and methodology; S. R.: formal analysis, methodology, and writing – review and editing; S. T.: conceptualization, supervision, and writing – review and editing; H. H.: conceptualization, supervision, project administration, and writing – original draft.

Conflicts of interest

There are no conflicts to declare.

Acknowledgements

This work was partly supported by the JSPS KAKENHI Grant Number JP23K04693.

References

1 W. I. F. David, *Appl. Radiat. Isot.*, 1995, **46**, 519–524.
2 Y. Jin, A. Xenopoulos, J. Cheng, W. Chen, B. Wunderlich, M. Diack, C. Jin, R. L. Hettich, R. N. Compton and G. Guiochon, *Mol. Cryst. Liq. Cryst. Sci. Technol., Sect. A*, 1994, **257**, 235–250.
3 G. Burns, F. H. Dacol and B. Welber, *Solid State Commun.*, 1979, **32**, 151–155.
4 M. Debeau and P. Depondt, *J. Chim. Phys.*, 1985, **82**, 233–238.
5 S. Ganguly Somnath, J. R. Fernandes and C. N. R. Rao, *Adv. Mol. Relax. Interact. Processes*, 1981, **20**, 149–163.
6 K. Kobashi and R. D. Etters, *Mol. Phys.*, 1982, **46**, 1077–1083.
7 J. Timmermans, *J. Phys. Chem. Solids*, 1961, **18**, 1–8.
8 H. Sakaebe and H. Matsumoto, *Electrochem. Commun.*, 2003, **5**, 594–598.
9 H. Usui, H. Matsui, N. Tanabe and S. Yanagida, *J. Photochem. Photobiol., A*, 2004, **164**, 97–101.
10 W. A. Henderson and S. Passerini, *Chem. Mater.*, 2004, **16**, 2881–2885.
11 T. Sato, T. Maruo, S. Marukane and K. Takagi, *J. Power Sources*, 2004, **138**, 253–261.
12 M. Egashira, S. Okada, J. Yamaki, D. A. Dri, F. Bonadies and B. Scrosati, *J. Power Sources*, 2004, **138**, 240–244.
13 M. Yoshizawa-Fujita, H. Yamada, S. Yamaguchi, H. Zhu, M. Forsyth, Y. Takeoka and M. Rikukawa, *Batteries Supercaps*, 2020, **3**, 884–891.
14 M. Matsuki, T. Yamada, S. Dekura, H. Kitagawa and N. Kimizuka, *Chem. Lett.*, 2018, **47**, 497–499.
15 C. Shi, S. Li, W. Zhang, L. Qiu and F. Yan, *J. Mater. Chem. A*, 2013, **1**, 13956–13962.
16 A. Martinelli, A. Matic, P. Jacobsson and L. Börjesson, *J. Phys. Chem. B*, 2009, **113**, 11247–11251.
17 L. Zhang, L. Chai, L. Zhang, M. Shen, X. Zhang, V. S. Battaglia, T. Stephenson and H. Zheng, *Electrochim. Acta*, 2014, **127**, 39–44.
18 S. Ferrari, E. Quartarone, P. Mustarelli, A. Magistris, M. Fagnoni, S. Protti, C. Gerbaldi and A. Spinella, *J. Power Sources*, 2010, **195**, 559–566.
19 M. Nádherná, J. Reiter, J. Moskon and R. Dominko, *J. Power Sources*, 2011, **196**, 7700–7706.
20 I. Quinzeni, S. Ferrari, E. Quartarone, C. Tomasi, M. Fagnoni and P. Mustarelli, *J. Power Sources*, 2013, **237**, 204–209.
21 L. Aguilera, J. Scheers and A. Matic, *Phys. Chem. Chem. Phys.*, 2016, **18**, 25458–25464.
22 D. R. MacFarlane and M. Forsyth, *Adv. Mater.*, 2001, **13**, 957–966.
23 M. Kenmotsu, H. Honda, H. Ohki, R. Ikeda, T. Erata, A. Tasaki and Y. Furukawa, *Z. Naturforsch.*, 1994, **49a**, 247–252.
24 H. Honda, M. Kenmotsu, H. Ohki, R. Ikeda and Y. Furukawa, *Ber. Bunsenges. Phys. Chem.*, 1995, **99**, 1009–1014.
25 H. Honda, S. Ishimaru, N. Onoda-Yamamuro and R. Ikeda, *Z. Naturforsch.*, 1995, **50a**, 871–875.

26 T. Hayasaki, S. Hirakawa and H. Honda, *Bull. Chem. Soc. Jpn.*, 2013, **86**, 993–1001.
27 T. Hayasaki, S. Hirakawa and H. Honda, *Am. Chem. Sci. J.*, 2014, **4**, 745–758.
28 T. Hayasaki, S. Hirakawa and H. Honda, *Z. Naturforsch.*, 2014, **69a**, 433–440.
29 S. Hirakawa and H. Honda, *Z. Naturforsch.*, 2015, **70**, 521–528.
30 Y. Kotani and H. Honda, *Bull. Chem. Soc. Jpn.*, 2019, **92**, 768–778.
31 K. Nagai and H. Honda, *Z. Naturforsch., A: Phys. Sci.*, 2022, **77**, 899–908.
32 S. Hirakawa, Y. Kotani, T. Hayasaki and H. Honda, *Bull. Chem. Soc. Jpn.*, 2015, **88**, 1735–1745.
33 Y. Yamada, E. Kashimoto and H. Honda, *Bull. Chem. Soc. Jpn.*, 2019, **92**, 1289–1298.
34 A. Abouimrane, P. Alarco, Y. Abu-Lebdeh, I. Davidson and M. Armand, *J. Power Sources*, 2007, **174**, 1193–1196.
35 R. E. A. Dillon and D. F. Shriver, *Chem. Mater.*, 1999, **11**, 3296–3301.
36 *Principles of Magnetic Resonance*, ed. C. P. Slichter, Springer-Verlag, New York, 3rd edn, 1992.
37 *Nuclear Magnetic Resonance and Relaxation*, ed. B. Cowan, Cambridge University Press, Cambridge, 1997.
38 *Transient Techniques in NMR of Solids*, ed. B. C. Gerstein, C. R. Dybowski, Academic Press, London, 1985.
39 G. W. Buchanan, *Prog. Nucl. Magn. Reson. Spectrosc.*, 1999, **34**, 327–377.
40 T. Pietrass and P. K. Burkert, *Magn. Reson. Chem.*, 1993, **31**, 709–713.
41 G. Buchanan, M. Gerzain and C. Ratcliffe, *Canadian J. Chem.*, 1999, 77, 1911–1921.
42 K. Gotoh, S. Kunimitsu, H. Zhang, M. M. Lerner, K. Miyakubo, T. Ueda, H. Kim, Y. Han and H. Ishida, *J. Phys. Chem. C*, 2018, **122**, 10963–10970.
43 *Plastistically Crystalline State*, ed. J. N. Sherwood, John Willy & Sons, New York, 1979.
44 R. E. A. Dillon, C. L. Stern and D. F. Shriver, *Solid State Ionics*, 2000, **133**, 247–255.
45 R. M. Izatt, J. S. Brashaw, S. A. Nielsen, J. D. Lamb, J. J. Christensen and D. Sen, *Chem. Rev.*, 1985, **85**, 271–339.
46 P. C. Barbosaa, M. M. Silva, M. J. Smith, A. Goncalves, E. Fortunato, S. C. Nunes and V. Z. Bermudez, *Electrochim. Acta*, 2009, **54**, 1002–1009.
47 A. Swiderska-Mocek and D. Naparstek, *Solid State Ionics*, 2014, **267**, 32–37.
48 L. Aguilera, J. Scheers and A. Matic, *Phys. Chem. Chem. Phys.*, 2016, **18**, 25458–25464.
49 M. Moriya, D. Kato, W. Sakamoto and T. Yogo, *Chem. Commun.*, 2011, **47**, 6311–6313.
50 K. Yang, Z. Liao, Z. Zhang, L. Yang. and S. Hirano, *Mater. Lett.*, 2019, **236**, 554–557.
51 S. Li, K. Yang, Z. Zhang, L. Yang and S. Hirano, *Ind. Eng. Chem. Res.*, 2018, **57**, 13608–13614.
52 L. Jin, P. C. Howlett, J. M. Pringle, J. Janikowski, M. Armand, D. R. MacFarlane and M. Forsyth, *Energy Environ. Sci.*, 2014, **7**, 3352–3361.
53 G. M. Sheldrick, *Acta Crystallogr., Sect. A: Found. Adv.*, 2015, **71**, 3–8.
54 G. M. Sheldrick, *Acta Crystallogr., Sect. A: Found. Crystallogr.*, 2008, **64**, 112–122.
55 G. M. Sheldrick, *Acta Crystallogr., Sect. C: Struct. Chem.*, 2015, **71**, 3–8.